Simulations of nano-separated charged surfaces reveal water reorientation and non-additivity of hydration and electrostatic repulsion

Alexander Schlaich,[*,†] Alexandre P. dos Santos,[‡] and Roland R. Netz[*,‡]

†*Laboratoire Interdisciplinaire de Physique, CNRS and Université Grenoble Alpes, UMR CNRS 5588, 38000 Grenoble, France*

‡*Fachbereich Physik, Freie Universität Berlin, Arnimallee 14, 14195 Berlin, Germany*

¶*Instituto de Física, Universidade Federal do Rio Grande do Sul, CEP 91501-970, 15051 Porto Alegre, Brazil*

E-mail: alexander.schlaich@univ-grenoble-alpes.fr; rnetz@physik.fu-berlin.de

Abstract

We perform atomistic simulations of nanometer-separated charged surfaces in the presence of monovalent counterions at fixed water chemical potential. The counterion density profiles are well described by a modified Poisson-Boltzmann (MPB) approach that accounts for non-electrostatic ion-surface interactions, while the effects of smeared-out surface-charge distributions and dielectric profiles are relatively unimportant. The simulated surface interactions are for weakly charged surfaces well described by the additive contributions of hydration and MPB repulsions, but already for a moderate surface density of $\sigma = -0.77$ e/nm^2 this additivity breaks down, which we rationalize by a modification of the hydration repulsion due to interfacial water reorientation.

Keywords

Charged surfaces, hydration repulsion, modified Poisson-Boltzmann theory, ion distributions, surface interactions, water orientation.

Many biologically and industrially relevant surfaces are charged in water, classical examples are lipid membranes[1–3], ionic surfactant layers[4] and solid surfaces such as glass, silica or mica[5–8]. The experimental and theoretical descriptions of the interaction between charged surfaces across aqueous electrolytes forms the foundation of colloidal science. The celebrated Poisson–Boltzmann (PB) theory[9] treats water as a dielectric continuum and becomes valid when surface charge density and ion valencies are low and thus ion correlations are negligible. According to PB theory the interaction pressure between similarly charged surfaces is always repulsive and decays exponentially for large surface separation, two predictions that are confirmed by numerous experiments[5–8].

Surface separations in the nanometer range have been investigated in experiments and simulations for systems such as silica[10–13], clay[14,15] or membrane stacks[16–20]. At such low surface separations an additional, exponentially decaying repulsive pressure contribution is present, which is similar to the hydration pressure found for soft polar surfaces with a zero net charge[16–19]. Experimental pressures between charged surfaces have been successfully fitted by assuming additivity of hydration and PB contributions[21–24]. However, such fits are of only limited persuasive power since the surface charge density and its location are mere fitting parameters.

Indeed, additional effects for nanometer surface separations suggest an essential modification of the traditional PB theory: i) Water confined in nanometer slabs exhibits dielectric properties distinctly different from bulk[25–28]. This is also suggested by a modified interfacial water structure inferred from non-linear spectroscopy[29–31]. ii) Surface charge distributions are neither laterally homogeneous nor sharply peaked normal to the surface, as typically assumed in PB modeling, but rather are discrete[32] and broadly distributed[25]. iii) Ions interact with charged as well as uncharged surface groups via ion-surface interactions which involve

surface-induced partial ion dehydration[33,34] and lead to ion-specific Hofmeister effects[35] and modifications of surface interactions[36]. iv) Finally, ion correlation effects, not included in PB theory, become relevant for highly charged surfaces and high ion valency, and make similarly charged walls attract each other[37], in strong contrast to the mean-field PB predictions.

Water-explicit simulations of charged surfaces in principle include all these effects and should thus allow for a crucial test of the assumption of additive hydration and PB pressures, in particular since the surface charge and its location are precisely known. Previous simulations reported ion density profiles between nanometer-separated charged surfaces[10–13,25]. However, technical difficulties to impose a constant water chemical potential, which is the experimentally realized ensemble, precluded so far the quantitative comparison of simulated surface pressures with theoretical predictions.

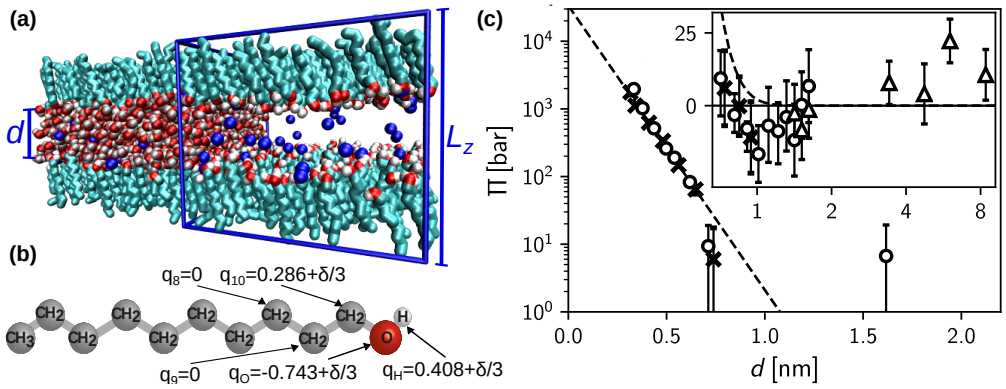

Figure 1: (a) Simulation snapshot for surface charge density $\sigma = -0.77\,\mathrm{e/nm^2}$ with $N_{\mathrm{ion}} = 18$ Na^+ ions and box height $L_z = 4.05\,\mathrm{nm}$, leading to a surface separation $d = 1.5\,\mathrm{nm}$. Water molecules are not shown in the central box. (b) Partial charge distribution on a decanol headgroup with a net charge δ. (c) Interaction pressure between neutral decanol surfaces for $N_d = 100$ (circles) and $N_d = 196$ decanols per surface (crosses). The dashed line is a fit of Eq. (6) to all positive pressure data yielding a decay length $\lambda = 0.10\,\mathrm{nm}$. In the large distance regime in the inset the pressure is zero within numerical accuracy. Triangles denote results for the equivalent osmotic pressure $\Pi = \Pi_0 + (\mu_{\mathrm{b}} - \mu)/v_{\mathrm{w}}^{\mathrm{b}}$ in the alternative $N_{\mathrm{w}} A \Pi_0 T$ ensemble for fixed $\Pi_0 = 1\,\mathrm{bar}$, see *Supplemental Material* for details.

In this paper we fix the water chemical potential by thermodynamic extrapolation methods[38,39], which we previously used for the study of the hydration repulsion between neutral lipid membranes[38], and compare simulated pressures between charged surfaces in the pres-

Table 1: Simulation parameters for neutral and charged surfaces. The coupling parameter Ξ is calculated using the SPC/E bulk dielectric constant $\varepsilon_{\rm b} = 70$[27].

δ	σ [e/nm^2]	Ξ	$N_{\rm ion}$	$L_x \times L_y$ [nm^2]	$N_{\rm d}$
0	0	-	-	4.83×4.83	100
0	0	-	-	6.77×6.77	196
-0.0255	-0.109	0.43	10	6.77×6.77	196
-0.09	-0.385	1.53	18	4.83×4.83	100
-0.18	-0.770	3.06	36	4.83×4.83	100

ence of monovalent counterions with theoretical predictions. For this we introduce a modified PB (MPB) theory that includes a general ion-surface interaction potential, an inhomogeneous dielectric profile and a smeared-out surface charge distribution. For low surface charge density we demonstrate that the total pressure is very accurately described by the sum of the MPB pressure and the hydration pressure, the latter being extracted from corresponding simulations between uncharged surfaces. But already for moderate surface charge densities of the order of 1 e/nm^2 this additive description breaks down. By analysis of the water orientation profile, which is significantly perturbed by surface charges, this break-down is suggested to be due to the attenuation of the effective hydration pressure. On the other hand, the counterion density profiles are still well described by the MPB theory, which suggests that ion correlation effects are unimportant at these surface charge densities (as corroborated by Monte Carlo simulations of water-implicit model systems). Our study suggests that water structural effects are crucial for the quantitative modeling of the interaction between charged surfaces at the nanoscale.

Methods. *Simulation model.* Our model surfaces consist of decanol bilayers with variable charges added to the head groups. Similar to experimental self-assembled monolayers (SAMs) on gold substrates, we fix the molecules on a centered rectangular lattice at a tilt angle of 30°, see Fig. 1 (a) for a snapshot. Two different lateral areas $A = L_x \times L_y$ with $N_{\rm d} = 100$ or 196 decanols per monolayers are studied, see Table 1 for parameters. The water number in the $N_{\rm w} A L_z T$ ensemble at constant temperature $T = 300\,{\rm K}$ is adjusted for each box height L_z such that the water chemical potential μ equals the bulk value $\mu_{\rm b} = -11.88\,{\rm kJ/mol}$[38].

For an accurate interaction pressure Π the error in μ has to be below $0.01\,k_{\mathrm{B}}T$, requiring at least $6\,\mu s$ simulation time per data point. Force-field parameters are based on GROMOS53A6[40] where the decanol hydroxyl groups are represented in atomistic detail, CH_2 and CH_3 groups as united atoms. The SPC/E water model is employed[41] and Na^+ parameters are taken from Ref.[42]. The repulsion between headgroup oxygens is increased to reduce intra-surface hydrogen bonding[43]. We consider counterions only so that the ion number N_{ion} is determined by total charge neutrality. All simulations are performed using version 5.0 of the GROMACS simulation package[44] with periodic boundary conditions. Lennard–Jones interactions are truncated and shifted at $r_{\mathrm{c}} = 0.9\,\mathrm{nm}$, for the electrostatic interactions the Particle Mesh Ewald method[45] is employed. As shown in the united atom representation of decanol in Fig. 1 (b), a negative charge of up to $\delta = -0.18$ is evenly distributed over the three COH-headgroup atoms, producing surface charge densities up to $\sigma = -0.77\,\mathrm{e/nm^2}$. Such a homogeneous surface charge distribution prevents specific ion binding and can experimentally be realized by potentiometric SAM setups[46–51]. The electrostatic coupling parameter in Table 1, defined by $\Xi = 2\pi q^3 \ell_{\mathrm{B}}^2 \sigma/e$ with the Bjerrum length $\ell_{\mathrm{B}} = e^2/(4\pi\varepsilon_0\varepsilon_{\mathrm{b}}k_{\mathrm{B}}T)$, is rather small and in a range where deviations from PB theory are moderate[52]. Our choice of a polar surface ensures that even for vanishing net charge the water slab is stable. For simulation details see the *Supplemental Material*.

Definition of surface charge position. When comparing simulations or experiments with PB models the surface charge distribution is important. Figure 2 (a) shows water and decanol oxygen density profiles for neutral and charged surfaces. Water density oscillations are absent since the surfaces are relatively soft[43,53]. The surface separation d is defined as the mean distance between decanol oxygen atoms in opposing layers. In Fig. 2 (b) we show the decanol charge density profile $\rho_{\mathrm{surf}}(z)$, which for the neutral surface (solid blue line) reveals a pronounced orientation of the OH headgroups. With increasing net surface charge $\sigma = \int_0^{L_z/2} \mathrm{d}z\, \rho_{\mathrm{surf}}(z)$ the surface charge profile shifts downwards. The plot of the excess surface charge profile $\Delta\rho_{\mathrm{surf}}(z) = \rho_{\mathrm{surf}}(z)|_{\sigma} - \rho_{\mathrm{surf}}(z)|_{\sigma=0}$ in Fig. 2 (c) demonstrates that d

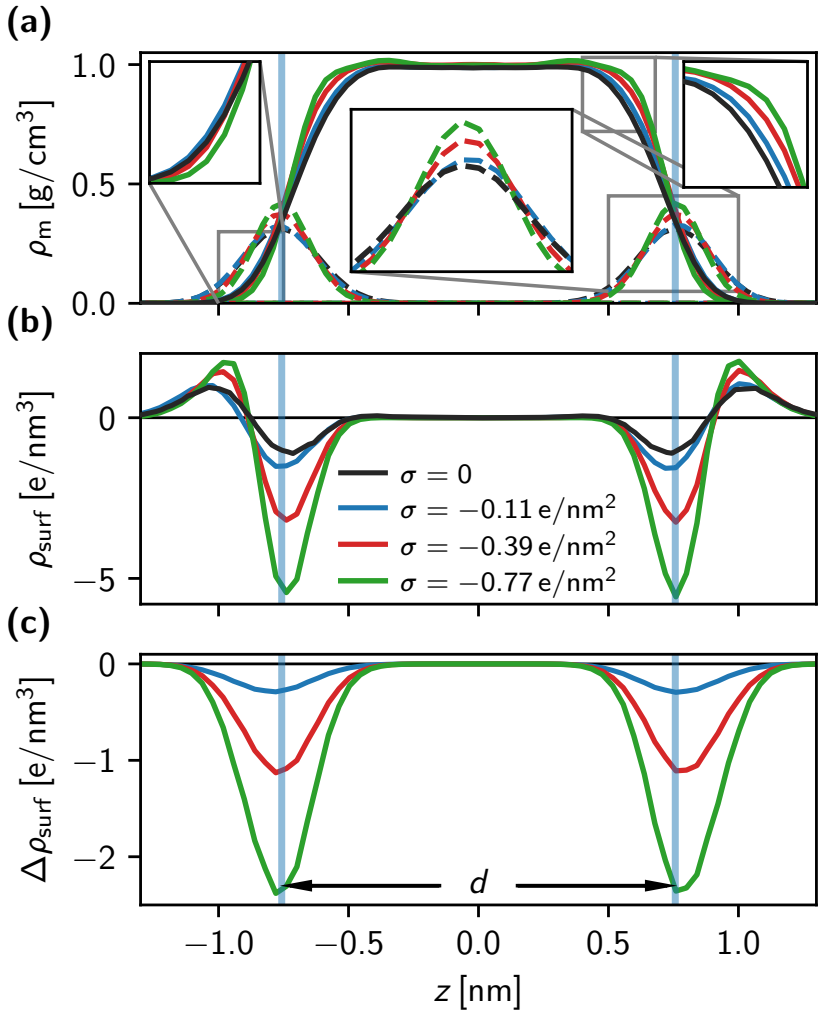

Figure 2: (a) Mass density ρ_m of water (solid lines) and decanol oxygens (dashed lines) for different surface charges σ at fixed box height $L_z = 4.05\,\text{nm}$. Vertical lines denote the surface position given by the separation $d = 1.51$ nm which follows from the mean decanol oxygen separation and differs by less than 0.02 nm for different σ. (b) Decanol charge density $\rho_{surf}(z)$. (c) Excess surface charge density $\Delta\rho_{surf}(z)$.

equals the distance between the excess charge maxima quite accurately, we therefore use d to characterize the surface charge position whenever needed.

Modified PB theory. The normal electric $E_\perp(z)$ and displacement fields $D_\perp(z)$ are related by the nonlocal inverse perpendicular dielectric function $\varepsilon^{-1}_{\mathrm{nl},\perp}$ according to

$$E_\perp(z) = \varepsilon_0^{-1} \int \mathrm{d}z'\, \varepsilon^{-1}_{\mathrm{nl},\perp}(z,z') D_\perp(z'), \tag{1}$$

where we used lateral homogeneity and averaged over the xy coordinates. For slowly varying $D_\perp(z)$ (i.e. for low σ) a systematic gradient expansion yields to leading order

$$E_\perp(z) = \varepsilon_0^{-1} \varepsilon_\perp^{-1}(z) D_\perp(z) \tag{2}$$

with the dielectric profile defined as $\varepsilon_\perp^{-1}(z) = \int \mathrm{d}z' \varepsilon^{-1}_{\mathrm{nl},\perp}(z,z')$. Defining the electrostatic potential $\Psi(z)$ by $\mathrm{d}\Psi(z)/\mathrm{d}z = -E_\perp(z)$ the mean-field counterion density distribution reads

$$\rho_{\mathrm{ion}}(z) = -qec_0 e^{-q\mathrm{e}\Psi(z)/k_\mathrm{B}T + U(z)}, \tag{3}$$

where $q = 1$ is the counterion valence and the potential $U(z)$ accounts for interfacial effects not included in the electrostatic potential $\Psi(z)$. The factor c_0 ensures that the total charge is zero, $\int_{-L_z/2}^{L_z/2} \mathrm{d}z\, \rho_{\mathrm{ion}}(z) \stackrel{!}{=} 2\sigma$. The displacement field is due to the sum of ion and surface charges according to

$$\frac{\mathrm{d}D_\perp(z)}{\mathrm{d}z} = \rho(z) = \rho_{\mathrm{ion}}(z) + \rho_{\mathrm{surf}}(z). \tag{4}$$

Combining the derivative of Eq. (2) with Eqs. (3) and (4) results in the integro-differential MPB equation[54–56] which is numerically solved (see *Supplemental Material*).

Results and Discussion. *Ion density profiles.* The simulated ion density profiles for different surface charge densities σ and different separations d are shown as blue lines in Fig. 3. The predictions from standard PB theory, using a constant bulk dielectric profile $\varepsilon_\perp^{-1}(z) = \varepsilon_\mathrm{b}^{-1}$, vanishing ion-surface interactions $U(z) = 0$ and sharply localized surface

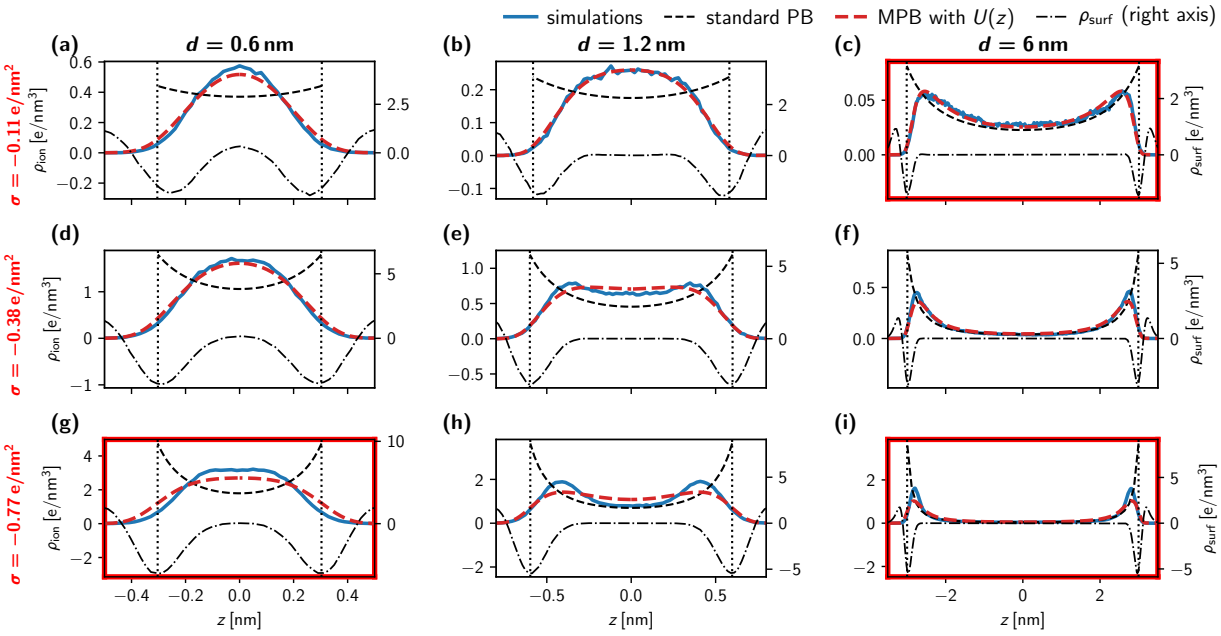

Figure 3: Simulation results for the ion density $\rho_{\text{ion}}(z)$ (solid blue lines) for different surface separations d (columns) and surface charge densities σ (rows). Dashed black lines show the standard PB prediction with the surface charge positions indicated by vertical dashed lines at $\pm d/2$, red dashed lines the MPB predictions including an ion-surface repulsion $U(z)$ according to Eq. (5). The dashed-dotted black lines show the surface-charge profiles $\rho_{\text{surf}}(z)$ (right axis). Results highlighted by red boxes are discussed in more detail in Fig. 4.

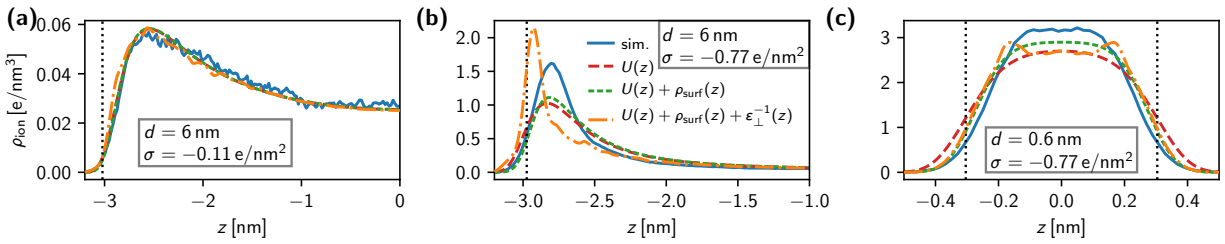

Figure 4: Simulation results for the ion density $\rho_{\text{ion}}(z)$ (solid blue lines) are for a few selected values of d and σ compared with MPB predictions including only the ion-surface interaction $U(z)$ (red broken line), $U(z)$ and the surface charge distribution $\rho_{\text{surf}}(z)$ (green dotted line), $U(z)$, $\rho_{\text{surf}}(z)$ and the dielectric profile $\varepsilon_\perp^{-1}(z)$ (orange dashed-dotted line). Vertical dashed lines indicate the mean surface-charge positions $\pm d/2$.

charges $\rho_{\mathrm{surf}}(z) = \delta\left(|z| - d/2\right)\sigma$, are shown as dashed black lines (see *Supplemental Material* for details). For the lowest surface charge $\sigma = -0.11\,\mathrm{e/nm^2}$ and large separation $d = 6\,\mathrm{nm}$ in Fig. 3 (c) the two profiles agree well apart from the interfacial region. However, for smaller separations in Fig. 3 (a) and (b) the standard PB model obviously fails.

We now turn to the MPB that features an exponential repulsive ion-surface interaction of the form

$$U(z) = a \exp\left(\frac{z - d/2}{\xi}\right) + a \exp\left(\frac{-z - d/2}{\xi}\right). \tag{5}$$

The decay length $\xi = (0.16 \pm 0.01)\,\mathrm{nm}$ and the potential strength $a = 2.7 \pm 0.1$ in units of $k_{\mathrm{B}}T$ are obtained from a fit of the MPB to the simulation data for $d > 1\,\mathrm{nm}$ at $\sigma = -0.11\,\mathrm{e/nm^2}$, see *Supplemental Material*. Using the same $U(z)$ with $\varepsilon_{\perp}^{-1}(z) = \varepsilon_{\mathrm{b}}^{-1}$ and localized surface charges, the MPB results shown by dashed red lines in Fig. 3 describe the simulation data well for all separations and surface charges.

The MPB that additionally includes the surface charge distribution $\rho_{\mathrm{surf}}(z)$ extracted from simulations, shown as dashed-dotted black lines in Fig. 3, does not significantly change the results, as we demonstrate for selected distances and surface charges by dotted green lines in Fig. 4. This is not surprising since $\rho_{\mathrm{surf}}(z)$ is peaked in the region where the surface repulsion $U(z)$ is large.

We now check the influence of a dielectric profile $\varepsilon_{\perp}^{-1}(z)$, which we extract from polarization fluctuations for uncharged surfaces[27], see *Supplemental Material* for details. The MPB solution including the ion-surface potential $U(z)$, the surface charge distribution $\rho_{\mathrm{surf}}(z)$ and the dielectric profile $\varepsilon_{\perp}^{-1}(z)$ is shown as orange dashed-dotted lines in Fig. 4. For small surface charge and large separation in Fig. 4 (a), where linear dielectric theory is expected to be reliable, the influence of the dielectric profile on the predicted ion density is negligible, for the high surface charge densities in Fig. 4 (b) and (c), for which we show below that linear dielectric theory is not expected to work, including $\varepsilon_{\perp}^{-1}(z)$ does not improve the agreement with the simulation data. Thus, the MPB theory which only includes the ion-surface potential $U(z)$ reproduces the simulated ion density profiles very well, while additional effects due

to dielectric effects and surface charge distributions are negligible.

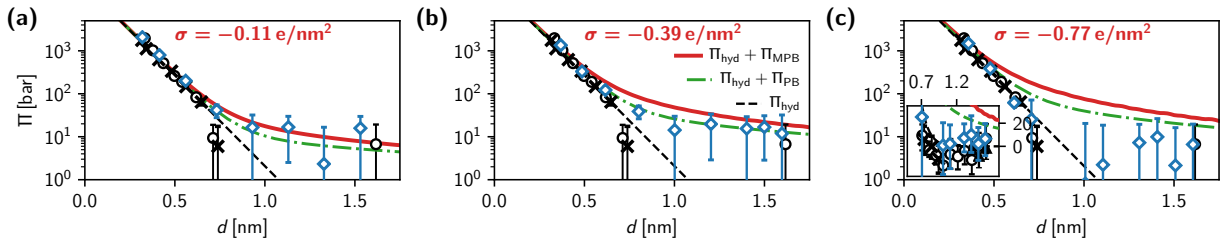

Figure 5: Simulated interaction pressures (blue diamonds) for three different surface charge densities σ are compared with results for uncharged surfaces (black symbols, including the exponential fit $\Pi_{\mathrm{hyd}}(z)$, Eq. (6), from Fig. 1 (c)) and the additive predictions $\Pi_{\mathrm{hyd}} + \Pi_{\mathrm{MPB}}$ (red lines) and $\Pi_{\mathrm{hyd}} + \Pi_{\mathrm{PB}}$ (green lines). The inset in (c) shows the data on a linear scale.

Interaction pressure. The simulated interaction pressure between charge-neutral polar surfaces in Fig. 1 (c) decays exponentially according to

$$\Pi_{\mathrm{hyd}} = \Pi^{\star} \mathrm{e}^{-d/\lambda} \tag{6}$$

with a decay length $\lambda = 0.10\,\mathrm{nm}$, and corresponds to the hydration repulsion[27,39,43,57]. The simulated pressures for finite surface charges are shown in Fig. 5 (blue diamonds) together with the neutral-surface result.

The MPB pressure follows from the free energy

$$\frac{\mathcal{F}_{\mathrm{MPB}}(d)}{A k_{\mathrm{B}} T} = -\frac{1}{2 k_{\mathrm{B}} T} \int_{-L_z/2}^{L_z/2} \rho(z) \Psi(z)\, \mathrm{d}z + \int_{-L_z/2}^{L_z/2} c(z) \left(\ln(c(z)) - 1\right)\, \mathrm{d}z + \int_{-L_z/2}^{L_z/2} U(z) c(z)\, \mathrm{d}z, \tag{7}$$

by differentiation, $\Pi_{\mathrm{MPB}}(d) = -\partial \mathcal{F}_{\mathrm{MPB}}(d)/(A \partial d)$. The first term in Eq. (7) is the electrostatic energy, the second accounts for the counterion entropy and the third results from ion–surface interactions, where $c(z) = \rho_{\mathrm{ion}}(z)/(qe)$ is the ion number density, see *Supplemental Material*.

In Fig. 5 we compare the simulated pressure to the sum of hydration and MPB pressures (red lines) and the sum of hydration and standard PB pressures (green broken lines). At low surface charge $\sigma = -0.11\,\mathrm{e/nm^2}$ in Fig. 5 (a), the simulation data is excellently described by $\Pi_{\mathrm{hyd}}+\Pi_{\mathrm{MPB}}$. The ion-surface repulsion $U(z)$ makes the MPB pressure slightly more repulsive compared to standard PB theory, but this difference is rather small, which is noteworthy in light of the pronounced differences between the MPB and PB ion density profiles in Fig. 3 (a)-(c). This reflects that the PB pressure for these small surface separations is essentially entropic and due to ion confinement, see *Supplemental Material* for details. The simulated pressures for $\sigma = -0.39\,\mathrm{e/nm^2}$ in Fig. 5 (b) are slightly smaller than $\Pi_{\mathrm{hyd}} + \Pi_{\mathrm{MPB}}$, for $\sigma = -0.77\,\mathrm{e/nm^2}$ in Fig. 5 (c) they are significantly smaller. This shows that the additivity assumption for hydration and MPB repulsive pressures breaks down already for moderate surface charge densities. These simulation results cannot be explained by ion correlation effects, as we demonstrate in the *Supplemental Material* by Monte Carlo (MC) simulations of counterions in a homogeneous dielectric medium between planar charged walls.

Water orientation at charged interfaces. The hydration repulsion is partly due to surface-induced water orientation effects[58–60]. In Fig. 6 we show profiles of the cosine of the orientation angle Θ between water dipoles and the surface normal. For neutral surfaces, $\sigma = 0$, water points with the oxygen towards the decanols due to favorable interaction with the surface hydrogens (solid black line). For weak surface charge $\sigma = -0.11\,\mathrm{e/nm^2}$ the orientation profile is not drastically changed, which explains the observed additivity of hydration and MPB pressures in Fig. 5 (a). For elevated surfaces charges $\sigma = -0.38$ and $-0.77\,\mathrm{e/nm^2}$ the water orientation changes profoundly and water hydrogens point to the surface due to the negative surface charge, in agreement with previous experiments and simulations[29–31,61,62]. This suggests that the failure of the pressure additivity assumption for $\sigma = -0.77\,\mathrm{e/nm^2}$ in Fig. 5 (c) results from a modification of the hydration force due to surface-charge induced water re-orientation. Note that MPB theory presumably still works even at high surface densities and low surface separations despite possible non-linear dielectric effects, since densities

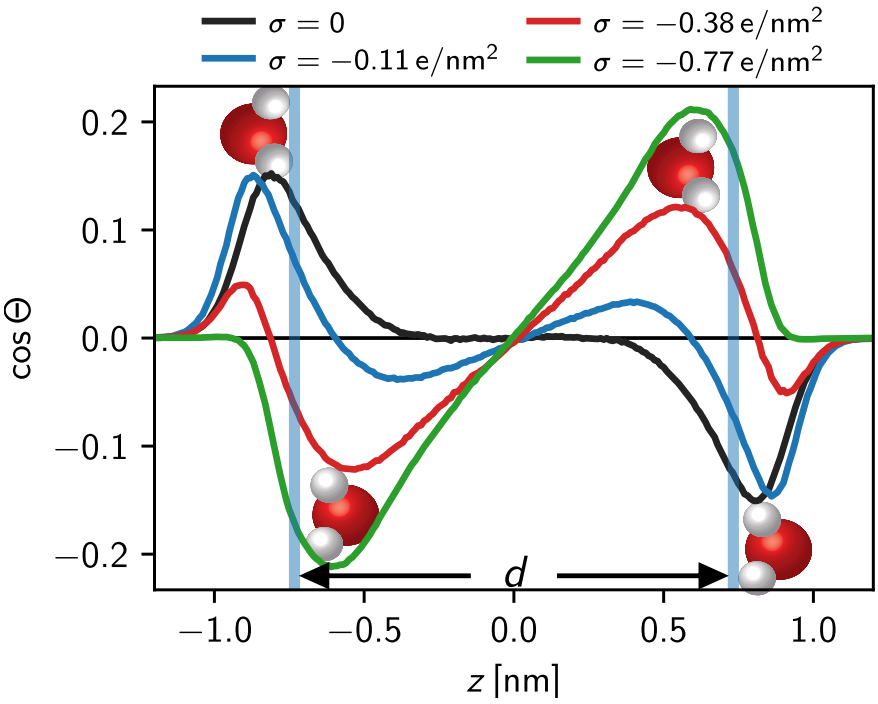

Figure 6: Water orientation profiles cos(Θ) for different surface charge densities σ at fixed surface separation $d = 1.5$nm.

and pressures are dominated by ion-confinement and not electrostatic effects. Interestingly, an increase of the surface charge also increases the water density close to the surface, as shown in Fig. 2 (a), which is correctly taken care of in our simulations by fixing the water chemical potential, see *Supplemental Material* for an in-depth discussion.

Conclusions. Our water-explicit simulations at fixed chemical potential show that monovalent counterion density profiles at soft charged surfaces are well described by a modified PB approach that includes non-electrostatic ion-surface interactions. The effects of dielectric profiles and smeared-out surface charge distributions are less important. At low surface charge densities our simulations confirm the additivity of hydration repulsion (extracted from simulations of uncharged surfaces) and surface-charge induced MPB pressure contributions down to sub-nanometer surface separations. However, already for a moderate surface charge density $\sigma = -0.77\text{e/nm}^2$ this additivity breaks down, which we rationalize by a modification of the hydration repulsion due to the surface-charge induced re-orientation of interfacial

water. That water reacts sensitively to the presence of surface charges is known from simulations and experiments[29–31,61,62], we show that this restructuring modifies the hydration repulsion and thus the effective surface interaction pressure significantly. Corrections to PB theory due to ion correlation effects, which have been extensively discussed[37], are relatively unimportant for moderate surface charge densities and monovalent couterions.

Acknowledgement

This work was supported by the European Innovative Training Network "Transport of Soft Matter at the Nanoscale" (NANOTRANS). A.d.S acknowledges funding from the Alexander von Humboldt Foundation through the CAPES program.

Supporting Information Available

The Supporting Material accompanying this manuscript includes: Further simulation details including the control of the water chemical potential, dielectric profiles, details on the MPB including a free energy decomposition, analytical solution of the PB equation between planar walls and results of the MC simulations.

Author information

Corresponding Author

Correspondence and requests for materials should be addressed to R.R.N.

Author contributions

A.S. and R.R.N. designed the research project; A.S. and A.d.S. performed simulations; A.S., A.d.S. and R.R.N. analyzed the data; A.S. and R.R.N. wrote the manuscript.

Notes

The authors declare no competing financial interests.

References

(1) Suetsugu, S.; Kurisu, S.; Takenawa, T. Dynamic Shaping of Cellular Membranes by Phospholipids and Membrane-Deforming Proteins. *Physiological Reviews* **2014**, *94*, 1219–1248.

(2) Leventis, P. A.; Grinstein, S. The Distribution and Function of Phosphatidylserine in Cellular Membranes. *Annual Review of Biophysics* **2010**, *39*, 407–427.

(3) Di Paolo, G.; De Camilli, P. Phosphoinositides in cell regulation and membrane dynamics. *Nature* **2006**, *443*, 651–657.

(4) Smulders, E.; von Rybinski, W.; Sung, E.; Rähse, W.; Steber, J.; Wiebel, F.; Nordskog, A. *Ullmann's Encyclopedia of Industrial Chemistry*; Wiley-VCH Verlag GmbH & Co. KGaA, 2000.

(5) Israelachvili, J. N.; Adams, G. Measurement of forces between two mica surfaces in aqueous electrolyte solutions in the range 0–100 nm. *Journal of the Chemical Society, Faraday Transactions 1: Physical Chemistry in Condensed Phases* **1978**, *74*, 975–1001.

(6) Pashley, R. M. DLVO and hydration forces between mica surfaces in Li+, Na+, K+, and Cs+ electrolyte solutions: A correlation of double-layer and hydration forces with surface cation exchange properties. *Journal of Colloid and Interface Science* **1981**, *83*, 531–546.

(7) Pashley, R. Hydration forces between mica surfaces in aqueous electrolyte solutions. *Journal of Colloid and Interface Science* **1981**, *80*, 153–162.

(8) Horn, R. G.; Smith, D. T.; Haller, W. Surface forces and viscosity of water measured between silica sheets. *Chemical Physics Letters* **1989**, *162*, 404–408.

(9) Andelman, D. In *Handbook of Biological Physics*; R. Lipowsky and E. Sackmann,, Ed.; Structure and Dynamics of Membranes; North-Holland, 1995; Vol. Volume 1; pp 603–642.

(10) Argyris, D.; Cole, D. R.; Striolo, A. Ion-Specific Effects under Confinement: The Role of Interfacial Water. *ACS Nano* **2010**, *4*, 2035–2042.

(11) Videla, P. E.; Sala, J.; Martí, J.; Guàrdia, E.; Laria, D. Aqueous electrolytes confined within functionalized silica nanopores. *The Journal of Chemical Physics* **2011**, *135*, 104503.

(12) Bonnaud, P. A.; Coasne, B.; Pellenq, R. J.-M. Solvated calcium ions in charged silica nanopores. *The Journal of Chemical Physics* **2012**, *137*, 064706.

(13) Ho, T. A.; Argyris, D.; Cole, D. R.; Striolo, A. Aqueous NaCl and CsCl Solutions Confined in Crystalline Slit-Shaped Silica Nanopores of Varying Degree of Protonation. *Langmuir* **2012**, *28*, 1256–1266.

(14) Bordallo, H. N.; Aldridge, L. P.; Churchman, G. J.; Gates, W. P.; Telling, M. T. F.; Kiefer, K.; Fouquet, P.; Seydel, T.; Kimber, S. A. J. Quasi-Elastic Neutron Scattering Studies on Clay Interlayer-Space Highlighting the Effect of the Cation in Confined Water Dynamics. *J. Phys. Chem. C* **2008**, *112*, 13982–13991.

(15) Malikova, N.; Longeville, S.; Zanotti, J.-M.; Dubois, E.; Marry, V.; Turq, P.; Ollivier, J. Signature of Low-Dimensional Diffusion in Complex Systems. *Phys. Rev. Lett.* **2008**, *101*, 265901.

(16) Parsegian, V.; Fuller, N.; Rand, R. Measured work of deformation and repulsion of

lecithin bilayers. *Proceedings of the National Academy of Sciences* **1979**, *76*, 2750–2754.

(17) Rand, R.; Parsegian, V. Hydration forces between phospholipid bilayers. *Biochimica et biophysica acta* **1989**, *988*, 351–376.

(18) Israelachvili, J. N.; Pashley, R. M. Molecular layering of water at surfaces and origin of repulsive hydration forces. *Nature* **1983**, *306*, 249–250.

(19) Marra, J.; Israelachvili, J. N. Direct measurements of forces between phosphatidylcholine and phosphatidylethanolamine bilayers in aqueous electrolyte solutions. *Biochemistry* **1985**, *24*, 4608–4618.

(20) Herrmann, L.; Johner, A.; Kékicheff, P. Interactions between Charged Lamellae in Aqueous Solution. *Phys. Rev. Lett.* **2014**, *113*, 268302.

(21) McIntosh, T. J.; Magid, A. D.; Simon, S. A. Interactions between charged, uncharged, and zwitterionic bilayers containing phosphatidylglycerol. *Biophys J* **1990**, *57*, 1187–1197.

(22) Parsegian, V. A.; Rand, R. P.; Fuller, N. L. Direct osmotic stress measurements of hydration and electrostatic double-layer forces between bilayers of double-chained ammonium acetate surfactants. *J. Phys. Chem.* **1991**, *95*, 4777–4782.

(23) Popa, I.; Sinha, P.; Finessi, M.; Maroni, P.; Papastavrou, G.; Borkovec, M. Importance of Charge Regulation in Attractive Double-Layer Forces between Dissimilar Surfaces. *Phys. Rev. Lett.* **2010**, *104*, 228301.

(24) Trefalt, G.; Palberg, T.; Borkovec, M. Forces between colloidal particles in aqueous solutions containing monovalent and multivalent ions. *Current Opinion in Colloid & Interface Science* **2017**, *27*, 9–17.

(25) Faraudo, J.; Bresme, F. Anomalous Dielectric Behavior of Water in Ionic Newton Black Films. *Phys. Rev. Lett.* **2004**, *92*, 236102.

(26) Bonthuis, D. J.; Gekle, S.; Netz, R. R. Dielectric Profile of Interfacial Water and its Effect on Double-Layer Capacitance. *Phys. Rev. Lett.* **2011**, *107*, 166102.

(27) Schlaich, A.; Knapp, E. W.; Netz, R. R. Water Dielectric Effects in Planar Confinement. *Phys. Rev. Lett.* **2016**, *117*, 048001.

(28) Fumagalli, L.; Esfandiar, A.; Fabregas, R.; Hu, S.; Ares, P.; Janardanan, A.; Yang, Q.; Radha, B.; Taniguchi, T.; Watanabe, K.; Gomila, G.; Novoselov, K. S.; Geim, A. K. Anomalously low dielectric constant of confined water. *Science* **2018**, *360*, 1339–1342.

(29) Dreier, L. B.; Nagata, Y.; Lutz, H.; Gonella, G.; Hunger, J.; Backus, E. H. G.; Bonn, M. Saturation of charge-induced water alignment at model membrane surfaces. *Science Advances* **2018**, *4*, eaap7415.

(30) Cyran, J. D.; Backus, E. H. G.; Nagata, Y.; Bonn, M. Structure from Dynamics: Vibrational Dynamics of Interfacial Water as a Probe of Aqueous Heterogeneity. *J. Phys. Chem. B* **2018**, *122*, 3667–3679.

(31) Hosseinpour, S.; Tang, F.; Wang, F.; Livingstone, R. A.; Schlegel, S. J.; Ohto, T.; Bonn, M.; Nagata, Y.; Backus, E. H. G. Chemisorbed and Physisorbed Water at the TiO2/Water Interface. *J. Phys. Chem. Lett.* **2017**, *8*, 2195–2199.

(32) Moreira, A. G.; Netz, R. R. Counterions at charge-modulated substrates. *Europhysics Letters (EPL)* **2002**, *57*, 911–917.

(33) Schwierz, N.; Netz, R. R. Effective Interaction between Two Ion-Adsorbing Plates: Hofmeister Series and Salting-In/Salting-Out Phase Diagrams from a Global Mean-Field Analysis. *Langmuir* **2012**, *28*, 3881–3886.

(34) Schwierz, N.; Horinek, D.; Netz, R. R. Specific Ion Binding to Carboxylic Surface Groups and the pH Dependence of the Hofmeister Series. *Langmuir* **2015**, *31*, 215–225.

(35) Jungwirth, P.; Tobias, D. J. Specific Ion Effects at the Air/Water Interface. *Chem. Rev.* **2006**, *106*, 1259–1281.

(36) Schwierz, N.; Horinek, D.; Netz, R. R. Anionic and Cationic Hofmeister Effects on Hydrophobic and Hydrophilic Surfaces. *Langmuir* **2013**, *29*, 2602–2614.

(37) Moreira, A. G.; Netz, R. R. Binding of Similarly Charged Plates with Counterions Only. *Phys. Rev. Lett.* **2001**, *87*, 078301.

(38) Schneck, E.; Sedlmeier, F.; Netz, R. R. Hydration repulsion between biomembranes results from an interplay of dehydration and depolarization. *PNAS* **2012**, *109*, 14405–14409.

(39) Kanduč, M.; Netz, R. R. From hydration repulsion to dry adhesion between asymmetric hydrophilic and hydrophobic surfaces. *PNAS* **2015**, *112*, 12338–12343.

(40) Oostenbrink, C.; Villa, A.; Mark, A. E.; Van Gunsteren, W. F. A biomolecular force field based on the free enthalpy of hydration and solvation: The GROMOS force-field parameter sets 53A5 and 53A6. *Journal of Computational Chemistry* **2004**, *25*, 1656–1676.

(41) Berendsen, H. J. C.; Grigera, J. R.; Straatsma, T. P. The missing term in effective pair potentials. *J. Phys. Chem.* **1987**, *91*, 6269–6271.

(42) Smith, D. E.; Dang, L. X. Computer simulations of NaCl association in polarizable water. *The Journal of Chemical Physics* **1994**, *100*, 3757–3766.

(43) Kanduč, M.; Schneck, E.; Netz, R. R. Attraction between hydrated hydrophilic surfaces. *Chemical Physics Letters* **2014**, *610–611*, 375–380.

(44) Abraham, M. J.; Murtola, T.; Schulz, R.; Páll, S.; Smith, J. C.; Hess, B.; Lindahl, E. GROMACS: High performance molecular simulations through multi-level parallelism from laptops to supercomputers. *SoftwareX* **2015**, *1–2*, 19–25.

(45) Essmann, U.; Perera, L.; Berkowitz, M. L.; Darden, T.; Lee, H.; Pedersen, L. G. A smooth particle mesh Ewald method. *The Journal of Chemical Physics* **1995**, *103*, 8577–8593.

(46) Hillier, A. C.; Kim, S.; Bard, A. J. Measurement of Double-Layer Forces at the Electrode/Electrolyte Interface Using the Atomic Force Mircoscope: Potential and Anion Dependent Interactions. *J. Phys. Chem.* **1996**, *100*, 18808–18817.

(47) Rentsch, S.; Siegenthaler, H.; Papastavrou, G. Diffuse Layer Properties of Thiol-Modified Gold Electrodes Probed by Direct Force Measurements. *Langmuir* **2007**, *23*, 9083–9091.

(48) Papastavrou, G. Combining electrochemistry and direct force measurements: from the control of surface properties towards applications. *Colloid Polym Sci* **2010**, *288*, 1201–1214.

(49) Kuznetsov, V.; Papastavrou, G. Ion Adsorption on Modified Electrodes as Determined by Direct Force Measurements under Potentiostatic Control. *J. Phys. Chem. C* **2014**, *118*, 2673–2685.

(50) Tivony, R.; Klein, J. Modifying surface forces through control of surface potentials. *Faraday Discuss.* **2017**, *199*, 261–277.

(51) Pashazanusi, L.; Oguntoye, M.; Oak, S.; Albert, J. N. L.; Pratt, L. R.; Pesika, N. S. Anomalous Potential-Dependent Friction on Au(111) Measured by AFM. *Langmuir* **2017**,

(52) Moreira, A. G.; Netz, R. R. Strong-coupling theory for counter-ion distributions. *Europhysics Letters (EPL)* **2000**, *52*, 705–711.

(53) Lorenz, C. D.; Lane, J. M. D.; Chandross, M.; Stevens, M. J.; Grest, G. S. Molecular Dynamics Simulations of Water Confined between Matched Pairs of Hydrophobic and Hydrophilic Self-Assembled Monolayers. *Langmuir* **2009**, *25*, 4535–4542.

(54) Boström, M.; Deniz, V.; Franks, G. V.; Ninham, B. W. Extended DLVO theory: Electrostatic and non-electrostatic forces in oxide suspensions. *Advances in Colloid and Interface Science* **2006**, *123-126*, 5–15.

(55) Paillusson, F.; Blossey, R. Slits, plates, and Poisson-Boltzmann theory in a local formulation of nonlocal electrostatics. *Phys. Rev. E* **2010**, *82*, 052501.

(56) Ben-Yaakov, D.; Andelman, D.; Podgornik, R.; Harries, D. Ion-specific hydration effects: Extending the Poisson-Boltzmann theory. *Current Opinion in Colloid & Interface Science* **2011**, *16*, 542–550.

(57) Kanduč, M.; Schlaich, A.; Schneck, E.; Netz, R. R. Water-Mediated Interactions between Hydrophilic and Hydrophobic Surfaces. *Langmuir* **2016**, *32*, 8767–8782.

(58) Marčelja, S.; Radić, N. Repulsion of interfaces due to boundary water. *Chemical Physics Letters* **1976**, *42*, 129–130.

(59) Cevc, G.; Podgornik, R.; Žekš, B. The free energy,enthalpy and entropy of hydration of phospholipid bilayer membranes and their difference on the interfacial separation. *Chemical Physics Letters* **1982**, *91*, 193–196.

(60) Kanduč, M.; Schlaich, A.; Schneck, E.; Netz, R. R. Hydration repulsion between membranes and polar surfaces: Simulation approaches versus continuum theories. *Adv. Colloid Interface Sci.* **2014**, *208*, 142–152.

(61) Du, Q.; Freysz, E.; Shen, Y. R. Vibrational spectra of water molecules at quartz/water interfaces. *Phys. Rev. Lett.* **1994**, *72*, 238–241.

(62) Dewan, S.; Carnevale, V.; Bankura, A.; Eftekhari-Bafrooei, A.; Fiorin, G.; Klein, M. L.; Borguet, E. Structure of Water at Charged Interfaces: A Molecular Dynamics Study. *Langmuir* **2014**, *30*, 8056–8065.

Graphical TOC Entry